ChemPubSoc Europe

DOI: 10.1002/cssc.201700237

CHEMSUSCHEM Full Papers

Operando Soft X-ray Absorption Spectroscopic Study on a Solid Oxide Fuel Cell Cathode during Electrochemical Oxygen Reduction

Takashi Nakamura,*[a] Ryo Oike,[a] Yuta Kimura,[a] Yusuke Tamenori,[b] Tatsuya Kawada,[c] and Koji Amezawa[a]

An operando soft X-ray absorption spectroscopic technique, which enabled the analysis of the electronic structures of the electrode materials at elevated temperature in a controlled atmosphere and electrochemical polarization, was established and its availability was demonstrated by investigating the electronic structural changes of an $La_2NiO_{4+\delta}$ dense-film electrode during an electrochemical oxygen reduction reaction. Clear O K-edge and Ni L-edge X-ray absorption spectra could be obtained below 773 K under an atmospheric pressure of 100 ppm O_2/He, 0.1 % O_2/He, and 1 % O_2/He gas mixtures. Considerable spectral changes were observed in the O K-edge X-ray absorption spectra upon changing the P_{O_2} and application of electrical potential, whereas only small spectral changes were observed in Ni L-edge X-ray absorption spectra. A pre-edge peak of the O K-edge X-ray absorption spectra, which reflects the unoccupied partial density of states of Ni 3d–O 2p hybridization, increased or decreased with cathodic or anodic polarization, respectively. The electronic structural changes of the outermost orbital of the electrode material due to electrochemical polarization were successfully confirmed by the operando X-ray absorption spectroscopic technique developed in this study.

Introduction

Energy conversion and storage applications, such as fuel cells, electrolysis cells, rechargeable batteries, and thermochemical and photochemical catalysts, have gained great attention as highly efficient and environmentally friendly technologies.[1–15] In these applications, mixed ionic and electronic conductors (MIECs) are widely used because of their high mixed ionic and electronic conductivity and high catalytic activity. To develop the above technologies, electrochemical, thermochemical, and photochemical reactions in the devices should be well understood. For this purpose, a direct observation technique, which is available under working conditions of the devices, that is, controlled temperature, atmosphere, and polarization conditions, is a strong tool. The development of operando measurement techniques, therefore, has been undertaken and demonstrated by many researchers.

Hard X-ray radiation is useful for operando observation because of its high permeability. For instance, the electrochemical reaction at the fuel cell electrode was studied by hard X-ray absorption spectroscopy.[16–18] The electronic and local structural changes of MIEC electrodes were analyzed from the 3d transition-metal K-edge in these studies. However, the 3d transition-metal K-edge does not directly represent the electronic structure of the outermost orbital of the electrode material, since the X-ray absorption spectra at the 3d transition-metal K-edge mainly observes the excitation of a core electron from the 1s to 4p orbital. To evaluate the relation between the surface reactants and the electronic structure of the electrode material, spectroscopy using soft X-ray radiation is more suitable because the use of a soft X-ray core electron transition allows the investigation of the partial density of states (pDOS) of 3d transition metals and oxygen. For instance, by using soft X-ray absorption spectroscopy, the absorption at the 3d transition-metal L-edge (excitation from 2p to 3d) and oxygen K-edge (excitation from 1s to 2p) can be evaluated. The X-ray absorption at 3d transition-metal L-edge and oxygen K-edge spectra represent the unoccupied pDOS of the transition-metal 3d orbital and the oxygen 2p orbital, respectively, which form the highest occupied molecular orbitals and the lowest unoccupied molecular orbitals, so-called HOMOs and LUMOs of conventional MIECs. Electrons and holes in the LUMO and HOMO directly interact with the reactants on the material surface. Therefore, interaction between the transition-metal 3d, oxygen 2p, gas molecules, and surface adsorbates should be clarified to understand reactions involving gas molecules such as water splitting, CO_2 reduction, and oxygen reduction/evolution reactions. However, the presence of gas molecules in the atmosphere makes the usage of soft X-rays for the operando obser-

[a] Dr. T. Nakamura, R. Oike, Dr. Y. Kimura, Dr. K. Amezawa
Institute of Multidisciplinary Research for Advanced Materials
Tohoku University
2-1-1 Katahira, Aoba-ku, Sendai, 980–8577 (Japan)
E-mail: t-naka@tagen.tohoku.ac.jp

[b] Dr. Y. Tamenori
Japan Synchrotron Radiation Institute
1-1-1, Kouto, Sayo-cho, Sayo-gun, Hyogo 679–5198 (Japan)

[c] Dr. T. Kawada
Graduate School of Environmental Studies, Tohoku University
6-6-1 Aramaki-Aoba, Aoba-ku, Sendai 980–8579 (Japan)

Supporting Information and the ORCID identification number(s) for the author(s) of this article can be found under http://dx.doi.org/10.1002/cssc.201700237.

vation challenging because of the poor permeability of soft X-rays. Such technical difficulties are being solved and in situ and operando observation techniques are being developed, which are available under a near-ambient pressure atmosphere and for aqueous solution containing systems.[19–25] Chueh and co-workers developed "ambient" pressure soft X-ray photoelectron and X-ray absorption spectroscopy (XPS and XAS, respectively) and successfully evaluated the water-splitting reaction and the oxygen-reduction reaction on MIEC electrodes at high temperatures under 0.1–1 Torr (13.3–133 Pa) pressures.[19–21] Crumlin et al. evaluated the surface chemistry and the electronic structure of the heterostructure fuel cell electrodes under a polarized state by soft X-ray XPS at 10^{-3} atm (~0.1 kPa) of pressure.[22] Whereas the measurement conditions were limited in a low pressure atmosphere, these studies successfully gave a new insight into the electrochemical reactions. For the development of real in situ and operando observations, a truly ambient pressure measurement technique is quite important.

We have previously established in situ soft X-ray absorption and emission spectroscopic techniques that enable soft X-ray absorption spectroscopy under a controlled gas atmosphere and at high temperatures to be carried out. The advantage of our technique is that the measurement can be performed under an atmospheric pressure, that is, 1 bar of total pressure, of He-based gas while controlling the partial oxygen pressure. By using this technique, Co L_{II}- and L_{III}-edges and O K-edge X-ray absorption and emission spectra of $LaCoO_3$-based oxides, typical cathode materials for solid oxide fuel cells, were successfully evaluated at room temperature to 873 K under $P_{O_2} = 10^{-2}$ to 10^{-4} bar.[26,27] In this study, we have further developed the operando soft X-ray absorption spectroscopic technique that is available under a controlled 1 bar gas atmosphere at high temperature and under an electrochemical polarization state. By the operando observation technique, one can unveil the detailed electronic structural changes during the electrochemical reaction and their influences on the reaction processes. Therefore, the technique is effective for a further understanding of the electrochemical reaction under device operating conditions. As a demonstration of this technique, the electrochemical oxygen reduction reaction on a $La_2NiO_{4+\delta}$ dense-film electrode was studied. $La_2NiO_{4+\delta}$-based oxides were chosen as model solid oxide fuel cell cathodes because they are considered as promising cathode materials as a result of their high mixed oxide ionic and electronic conductivity and catalytic activity.[28–30]

Results and Discussion

Figure 1 shows the schematic illustration and pictures of the electrochemical cell, as well as the sample holder for the operando measurement. The electrochemical cell was located on a Pt–Ir heater located inside a Dewar vessel. A large part of the sample, except for the X-ray irradiation area was coated by heat-insulating cement, to reduce the heat radiation and keep the temperature. A Pt–PtRh thermocouple (TC) was placed adjacent to the $La_2NiO_{4+\delta}$ film electrode to monitor the sample

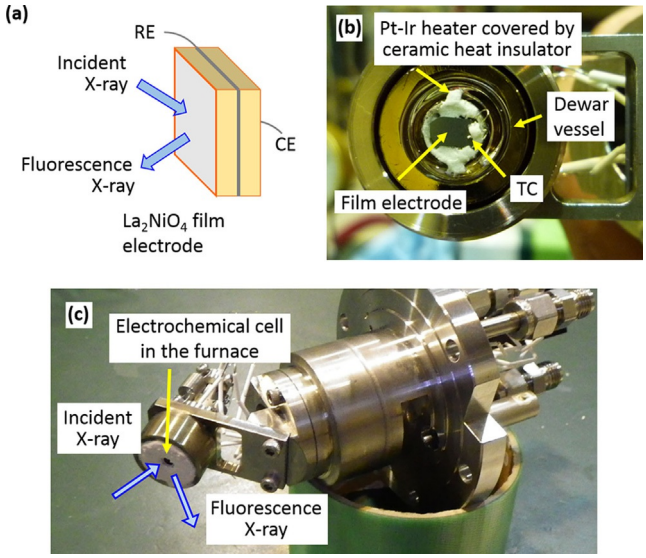

Figure 1. (a) Schematic image and (b) close-up view picture of the electrochemical cell, and (c) overview picture of the sample holder for operando soft X-ray absorption spectroscopy.

temperature accurately. The sample holder was fixed at the end chamber of the beam line.

Figure 2 shows the XRD pattern and SEM image of the $La_2NiO_{4+\delta}$ dense-film electrode obtained by the pulsed laser deposition (PLD) technique and powder specimen. The XRD pattern showed diffraction peaks of $La_2NiO_{4+\delta}$ and $Ce_{0.9}Gd_{0.1}O_{1.95}$ (GDC) substrate and no peaks from any other compound were detected. Compared with the powder diffraction pattern of $La_2NiO_{4+\delta}$ indexed by a tetragonal cell, (200) and (101) peaks were strongly enhanced, whereas (103), (110), and (114) peaks were weakened, which meant that the film obtained was polycrystalline and tended to be oriented to (100) in the out-of-plane direction. La_2NiO_4-based oxides have a crystal structure alternately connecting the rock salt and the perovskite structures in the direction of (001), and the ionic and electronic conduction paths are formed in the rock salt and the perovskite structures, respectively, along the (001) plane. Thus, smooth ionic and electronic conduction can be expected in the out-of-plane direction of the dense-film electrode prepared. From the SEM image given in Figure 2, the film was sufficiently dense and its thickness was about 700 nm. The film thickness was also confirmed by a surface profiler and consistent results were obtained.

Soft X-ray absorption spectroscopic measurements were first performed in 100 ppm O_2/He atmosphere by increasing the temperature from room temperature up to 773 K to check for an available optimum temperature for the operando measurements. The temperature dependence of O K-edge and Ni L-edge X-ray absorption spectra is summarized in Figure S1-1 (see the Supporting Information). Clear X-ray absorption spectra could be obtained at least up to 773 K. Therefore, the following measurements were carried out at 773 K. Figure 3 shows soft X-ray absorption spectra of the $La_2NiO_{4+\delta}$ film electrode obtained at 773 K in 100 ppm O_2/He, 0.1 %O_2/He, and 1 %O_2/He under open-circuit conditions. Peaks at around 849,

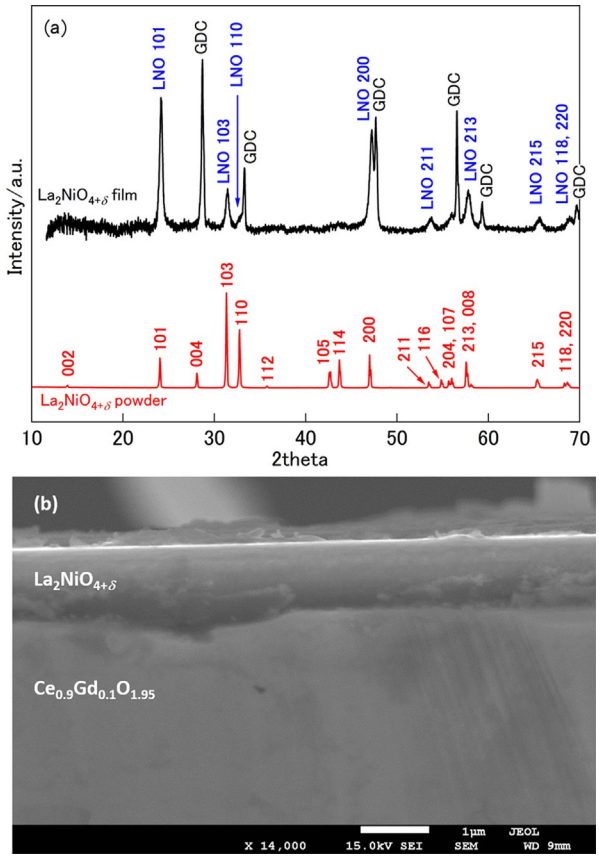

Figure 2. (a) XRD patterns of the $La_2NiO_{4+\delta}$ dense-film electrode on the $Ce_{0.9}Gd_{0.1}O_{1.95}$ electrolyte and $La_2NiO_{4+\delta}$ powder sample indexed by assuming tetragonal symmetry. (b) SEM image of the cross-section of the electrode/electrolyte interface.

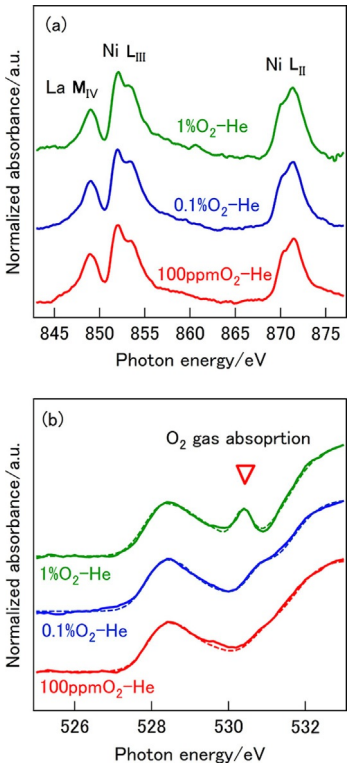

Figure 3. (a) Ni L-edge and (b) O K-edge X-ray absorption spectra of the $La_2NiO_{4+\delta}$ dense-film electrode measured by fluorescence yielding mode at 773 K under an atmospheric pressure of 100 ppm O_2/He, 0.1 % O_2/He, and 1 % O_2/He under open-circuit conditions. Dashed lines in (b) are the fitting results.

853, and 872 eV in Ni L-edge X-ray absorption spectra can be assigned to the La M_{IV}-edge, the Ni L_{III}-edge, and the Ni L_{II}-edge, respectively.[31–34] The Ni L-edge X-ray absorption spectra were normalized by the intensity change of the La M_{IV}-edge peak. Very minor spectral changes were observed at the shoulder of the L_{III}- and L_{II}-edges. In the O K-edge X-ray absorption spectra, the pre-edge peak below 530 eV corresponds e_g and t_{2g} hybridizations of Ni 3d and O 2p of the ligand oxygen, and the main absorption edge of the spectra was determined by the hybridization of the lanthanum and the lattice oxygen and the small contribution of the hybridization of Ni and the lattice oxygen.[31–34] O K-edge spectra in Figure 3 b were normalized by the change between the intensity at 533 eV and the base line below 526 eV. The spectra could be compared to evaluate the variation of electronic structures because the main absorption edge is mainly composed by the hybridization of La and O, and is almost invariant with the applied bias and/or the change in atmospheric conditions.

The absorption by oxygen molecules in the gas phase was detected at around 531 eV, which is indicated by a red triangle in Figure 3 b. The absorption by the oxygen gas became larger as P_{O_2} increased. Operando measurements were carried out in a 0.1 % O_2/He atmosphere at 773 K in this study so that the absorption by oxygen gas could be negligible. While this P_{O_2} condition is lower compared with that for the practical solid oxide fuel cell cathode, this new operando observation technique may provide information on the electronic structural changes of the electrode material during the electrochemical oxygen reduction reaction.

Figure 4 shows Ni L-edge and O K-edge X-ray absorption spectra measured at 773 K in 0.1 % O_2/He under cathodic and anodic polarization. Relaxation of the polarization currents under various bias conditions are summarized in Figure S1-2 (see the Supporting Information). The steady-state current showed slight fluctuations possibly due to a large impedance of the electrochemical cell, but was almost constant within the time scale of operando soft X-ray absorption measurements. While the change in Ni L-edge X-ray absorption spectra due to electrochemical polarization was very small, the intensity of the pre-edge peak at around 530 eV in the O K-edge X-ray absorption spectra increased with the cathodic bias and decreased with the anodic bias. Such changes of the absorption intensity depending on the applied bias suggest that electronic structures of the $La_2NiO_{4+\delta}$ dense film electrode were strongly affected by the electrochemical polarization. Since Ni 3d and O 2p forms the outermost orbital of $La_2NiO_{4+\delta}$, the spectral changes reflecting changes in the electronic states of Ni 3d and O 2p (Figure 4) are quite important when considering the electrochemical properties of the electrode material under electrochemical polarization.

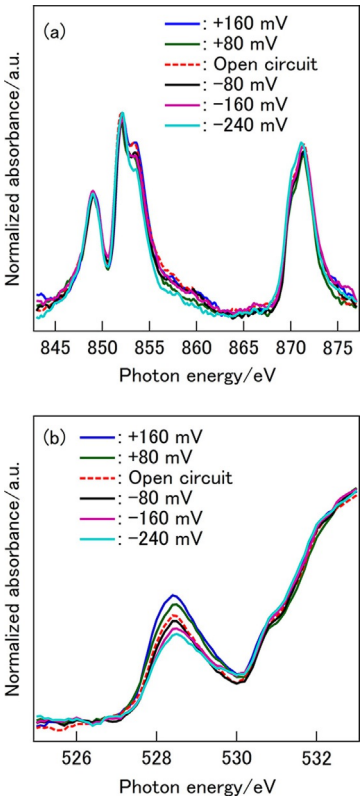

Figure 4. (a) Ni L-edge and (b) O K-edge X-ray absorption spectra of the $La_2NiO_{4+\delta}$ dense-film electrode measured by the fluorescence yielding mode at 773 K under an atmospheric pressure of 0.1 % O_2/He under anodic and cathodic polarization.

Before discussing the change of electronic structures of the La_2NiO_4 electrode from spectral changes in Ni L- and O K-edges X-ray absorption spectra, a brief reaction mechanism is summarized as follows: The reaction pathway of the electrochemical oxygen reduction in a dense MIEC electrode can be simplified compared with a typical porous electrode containing a complex 3D microstructure. In the case of a dense MIEC electrode, steady-state oxide ionic current flows through the surface processes, the ionic diffusion in the electrode, and the interface process in series. The oxygen reduction reaction process is depicted in Figure 5 a. In oxygen on the hypostoichiometric $La_2NiO_{4+\delta}$ film electrode, the (dissociative) adsorption of oxygen molecules, charge transfer to the surface oxygen species, and the incorporation of surface oxygen into the vacant interstitial site are the representative examples of surface processes.[35] Under open-circuit conditions, the oxygen chemical potential, μ_O, in the electrode was equilibrated with that in the gas phase. When an electrical potential was applied to the cell, the effective oxygen partial pressure at the electrode/electrolyte interface, $P_{O_2,int}$, which corresponds to the effective oxygen chemical potential at the interface, changes depending on the applied electrical potential to the electrode (=electrode overpotential) as follows:

$$P_{O_2,int} = P_{O_2,gas} + \exp\left(\frac{4F\Delta\eta}{RT}\right) \quad (1)$$

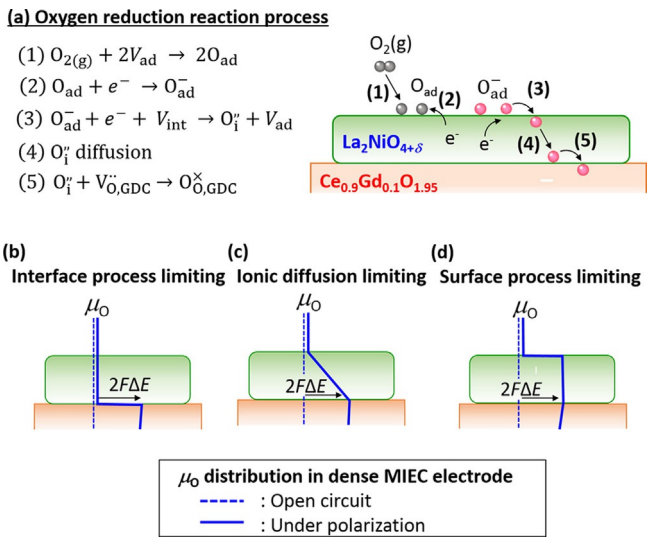

Figure 5. (a) Schematic illustration of the reaction steps for oxygen reduction on dense $La_2NiO_{4+\delta}$ film electrode. Oxygen chemical potential distribution under polarization,[35] (b) the interface process limiting case, (c) the diffusion limiting case, and (d) the surface process limiting case.

in which, $P_{O_2,gas}$, F, R, and $\Delta\eta$ are the oxygen partial pressure in the gas phase, the Faraday constant, the gas constant, and the applied electrical potential to the electrode, respectively. Equation (1) indicates that μ_O at the electrode/electrolyte interface can be controlled by changing P_{O_2} in the atmosphere and/or the applied electrical potential.[36] Since the gap of μ_O is the driving force for the electrochemical oxygen reduction and mainly consumed to promote the slowest process, a steep potential drop is formed at the position at which the rate-determining process is. Therefore, the μ_O distribution in the dense MIEC electrode under steady-state polarization conditions differs significantly depending on the rate-determining process.[36] Schematic images of the distribution of μ_O during the electrochemical oxygen reduction reaction are shown in Figure 5 assuming the local equilibrium. If some processes at the electrode/electrolyte interface determine the whole reaction rate, a sudden μ_O gap is formed at the electrode/electrolyte interface (Figure 5 b). If the bulk diffusion through the electrode layer is the rate-determining step, a μ_O gradient is formed in the film along the in-depth direction (Figure 5 c). If the surface reaction limits the whole reaction rate, a large μ_O gap is formed at the electrode surface (Figure 5 d). In the case of Figure 5 d, μ_O is uniform in the electrode and almost equal to that at the electrode/electrolyte interface.

As seen in Figure 4, minor changes in the Ni L-edge X-ray absorption spectra and considerable changes in the O K-edge X-ray absorption spectra were observed. These changes suggest that the change of electronic structures due to the electrochemical polarization was more significant in the 2p orbital of the ligand oxygen than in the 3d orbital of Ni. These spectral changes were quite similar to those of $La_2NiO_{4+\delta}$ when the concentration of interstitial oxygen changes.[36] In $La_2NiO_{4+\delta}$, the concentration of interstitial oxygen changes depending on P_{O_2} according to the following defect equilibrium

$$\frac{1}{2}O_2(g) + V_i^{\times} \rightarrow O_i^{\cdot\cdot} + 2h^{\cdot} \quad (2)$$

in which the defect species are denoted by Kröger–Vink notation. In the case of $La_2NiO_{4+\delta}$, holes (unoccupied pDOS) are created by the interstitial oxygen formation to keep charge neutrality. A pre-edge peak at around 530 eV of the O K-edge X-ray absorption spectra increased when increasing the interstitial oxygen concentration, and the change in the Ni L-edge X-ray absorption spectra was small. These spectral changes were interpreted in such a way that the charge transferred from the ligand oxygen to Ni, that is, holes introduced by the interstitial oxygen formation tended to localize to the 2p orbital of the ligand oxygen.[34] When the applied electrical potential changes the oxygen chemical potential in the electrode, the interstitial oxygen concentration in the $La_2NiO_{4+\delta}$ electrode also changes. Then, unoccupied pDOS changes due to hole creation were accompanied by the interstitial oxygen formation. Because soft X-ray absorption spectroscopy can detect the electronic structures only near the surface of the specimen, the results given in Figure 4, that is, the increase/decrease of unoccupied pDOS with cathodic/anodic bias, indicate that the applied electrical potential changed μ_O and the electronic structures near the surface of the electrode. The change of the defect and electronic structures can significantly affect the electrochemical activity and the surface kinetics.

For further insight into the change of electronic structures of $La_2NiO_{4+\delta}$ film electrode during electrochemical polarization, the O K-edge X-ray absorption spectra were fitted by a background line and five Gaussian curves. An arctangent curve was fitted as a background line according to earlier work.[37] Two Gaussian curves were fitted for the pre-edge peak as unoccupied pDOS of hybridization of Ni 3d–O 2p. According to earlier spectroscopic studies, the unoccupied pDOS of Ni 3d in $La_2NiO_{4+\delta}$ (Ni^{2+} d8 state: $t_{2g}^6e_g^2$) is composed of $d_{x^2-y^2}$, and $d_{z^2-r^2}$ owing to Jahn–Teller distortion of the NiO_6 octahedron.[31,34] One Gaussian curve was fitted for the absorption due to oxygen molecules in the gas phase and two Gaussian curves for the main absorption peak (La–O hybridization) and the contribution of Ni–O hybridization at the shoulder of the lower energy side. The calculated results are shown in Figures 3 and 6. The calculated curve seems consistent with observed X-ray absorption spectra. Integrated peak intensity of the pre-edge peak was calculated from the area of the two Gaussian curves for the pre-edge peak of O K-edge X-ray absorption spectra for the discussion of the electronic structural changes by the electrochemical polarization. A similar study was previously undertaken to evaluate the electronic structures of transition metal oxides from X-ray absorption spectra.[34,37,38] Since the integrated peak intensity represents an unoccupied pDOS of the oxygen 2p hybridized with Ni 3d, this can be a good indicator to understand the electronic structural changes of the electrode material under electrochemical polarization.

Figure 7 shows the integrated intensity of the pre-edge of the O K-edge X-ray absorption spectra as a function of $P_{O_2,int}$. The integrated peak intensity observed under polarization laid

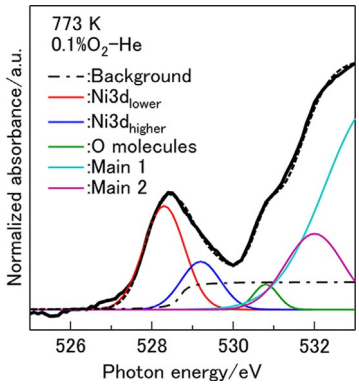

Figure 6. Fitting results of O K-edge X-ray absorption spectra. Dashed black line shows the sum of the background and the Gaussian curves.

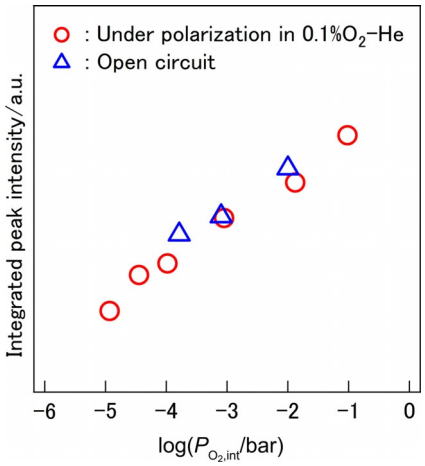

Figure 7. Integrated intensity of the pre-edge peak of the O K-edge X-ray absorption spectra under different atmospheric and bias conditions at 773 K plotted as a function of $P_{O_2,int}$ calculated by Equation (1).

on the same curve as that observed under various ambient P_{O_2} under open-circuit conditions. This means the oxygen chemical potential near the electrode surface under polarization is almost equal to that at the electrode/electrolyte interface. Therefore, it can be concluded that the electrochemical polarization induces the change of μ_O in the whole part of the electrode as shown in Figure 5 d. The results given in Figures 4 and 7 strongly suggested that an applied electrical potential induces the changes of the defect and electronic structures of the electrode, and the O 2p orbital contributes to the oxygen reduction/evolution reactions on an La_2NiO_4 film electrode. Contribution of the anion redox to electrochemical reactions is also suggested in some mixed ionic and electronic conducting oxides.[20,39,40]

A detailed reaction mechanism can be inferred from a systematic understanding of the electronic and defect structures of the electrode, surface chemical species, and electrochemical responses. In this study, we tried to combine the electrochemical properties and electronic structures of the electrode material. Electrochemical impedance spectroscopy (EIS) was carried out using the same electrochemical cell for the operando ob-

servation. Impedance spectra obtained under the same conditions with operando observation (0.1 % O_2 at 773 K) were not suitable for detailed analysis due to the large impedance of the electrochemical cell at relatively low temperature in a diluted oxygen atmosphere (Figure S2-1). Therefore, EIS measurements were carried out at 973 K at different P_{O_2} and bias conditions. The temperature difference between the operando observation and EIS measurements was also taken into account (see the Supporting Information, part S-2). Although the experimental conditions (temperature and atmosphere) were not completely the same, consistent results were obtained from EIS and XAS measurements, that is, a surface process is the rate-determining step for the oxygen reduction reaction on the $La_2NiO_{4+\delta}$ film electrode, and electrochemical polarization induced the change of the defect and electronic structures of an $La_2NiO_{4+\delta}$ electrode. Because the changes of the defect and electronic structures can significantly affect the electrochemical activity of the electrode, the contribution of such phenomena should be taken into account for further detailed analysis of the reaction mechanism.

The polarization resistance and steady-state current, which are considered to be determined by the slowest process at the electrode surface, are roughly proportional to $P_{O_2}{}^{-1/2 \text{ to } -1/4}$. This tendency is consistent with earlier work, which suggests that the dissociative adsorption of oxygen molecules or the charge transfer are possible candidates for the rate-determining step.[35,41,42] To elucidate the reaction mechanism, evaluating the activity dependence of the rate constants is a conventional and well-accepted method. However, this may not be effective when some processes are overlapped and the interaction between active species, defects, and electronic structures of the electrode is not negligible. In such a case, the operando measurement technique used in this study will be a powerful tool for providing information on the electronic structural changes during electrochemical reaction, as well as the electrochemical responses under different bias and atmospheric conditions. Although further developments are necessary, we could demonstrate the promising future of this new analytical technique for the elucidation of the reaction mechanisms by combining the electrochemical response and information of electronic and defect structures of the electrode during the reaction.

Conclusions

In this study, the operando soft X-ray absorption spectroscopic technique, which could be applied to the analysis of materials at elevated temperatures in controlled atmospheres under electrochemical polarization, was established, and its availability and effectiveness were demonstrated by evaluating the variation in electronic structures of an $La_2NiO_{4+\delta}$ dense-film electrode during electrochemical oxygen reduction. Clear O K-edge and Ni L-edge X-ray absorption spectra of the $La_2NiO_{4+\delta}$ film electrode could be obtained under a polarization state at 773 K in 100 ppm O_2/He, 0.1 % O_2/He, and 1 %O_2/He at atmospheric pressure. The increase/decrease in unoccupied pDOS of the outermost orbital, the hybridization of Ni 3d–O 2p, of a $La_2NiO_{4+\delta}$ dense-film electrode was observed during the oxygen reduction/evolution reaction. This strongly indicated that the electronic and defect structures were changed by electrochemical polarization and that such changes influenced the electrochemical activity of the electrode material.

Experimental Section

General

Commercial $Ce_{0.9}Gd_{0.1}O_{1.95}$ (GDC) powder (Shin-Etsu Chemical. Co., Ltd.) was pressed into a disc shape and sintered at 1823 K for 6 h. The dense polycrystalline GDC electrolyte was polished, and a $La_2NiO_{4+\delta}$ dense film was fabricated as a working electrode on one surface of the electrolyte by pulsed laser deposition. The GDC electrolyte was placed in a chamber filled with 10^{-6} bar O_2 and was heated at 923 K during the film fabrication. A $La_2NiO_{4+\delta}$ target was irradiated by a Nd-YAG pulsed laser of about 150 kJ cm^{-2} with a precision rate of 10 Hz. After the deposition, the film was heat-treated at 923 K for 9 h in 1 bar O_2 for crystallization. The crystallinity and morphology of the film were evaluated by X-ray diffraction measurements (D8 Discover, Bruker) and SEM observation (JSM-7001F, JEOL). The thickness of the film was also confirmed by the surface profiler (Dektak 150, Bruker). The specimen was cut into 4 × 4 mm squares and porous Pt electrodes were set on the opposite surface and the lateral side of the GDC electrolyte as counter and reference electrodes. Operando soft X-ray absorption spectroscopy was carried out at BL27SU, SPring-8, Japan. Atmospheric-pressure gas mixtures of O_2/He were introduced to the chamber to control oxygen partial pressure around the electrochemical cell. To ensure a high intensity of incident X-ray, the end chamber was separated from upstream chambers for the light pathway by a Si_3N_4 thin film window with 150 nm of thickness. The upstream chambers were evacuated by the differential pumping system.[43] Ni L_{II}- and L_{III}-edge (844–876 eV) and O K-edge (525–533 eV) X-ray absorption spectra under electrochemical polarization were recorded by the fluorescence yielding mode in order not to disturb the electrochemical measurement. EIS and steady-state polarization measurements were also carried out with the same electrochemical cell by a potentiostat (VersaStat 4, Princeton Applied Research).

Acknowledgements

This work was supported by CREST, JST (grant No. JPMJCR11C1) and JSPS Grant-in-Aid for Scientific Research No. 24656374. The synchrotron radiation experiments were performed at the BL27SU of SPring-8 with the approval of the Japan Synchrotron Radiation Research Institute (JASRI; Proposal Nos. 2013A1716, 2013B148, and 2014A1452).

Keywords: cathodes · electrochemistry · electronic structure · fuel cells · X-ray absorption spectroscopy

[1] N. Q. Minh, *J. Am. Ceram. Soc.* **1993**, *76*, 563 – 588.
[2] Z. Shao, S. M. Haile, *Nature* **2004**, *431*, 170 – 173.
[3] E. P. Murray, T. Tsai, S. A. Barnett, *Nature* **1999**, *400*, 649 – 651.
[4] Y. Singh, H. Muroyama, T. Matsui, S. Hashigami, T. Inagaki, K. Eguchi, *J. Power Sources* **2015**, *293*, 642 – 648.
[5] J. C. Ruiz-Morales, D. Marrero-López, J. Canales-Vázquez, J. S. T. Irvine, *RSC Adv.* **2011**, *1*, 1403 – 1414.
[6] T. Takeguchi, T. Yamanaka, H. Takahashi, H. Watanabe, T. Kuroki, H. Nakanishi, Y. Orikasa, Y. Uchimoto, H. Takano, N. Ohguri, M. Matsuda, T. Murota, K. Uosaki, W. Ueda, *J. Am. Chem. Soc.* **2013**, *135*, 11125 – 11130.

[7] K. N. Jung, J. H. Jung, W. B. Im, S. Yoon, K. H. Shin, J. W. Lee, *ACS Appl. Mater. Interfaces* **2013**, *5*, 9902 – 9907.
[8] P. Furler, J. R. Scheffe, A. Steinfeld, *Energy Environ. Sci.* **2012**, *5*, 6098 – 6103.
[9] C. K. Yang, Y. Yamazaki, A. Aydin, S. Haile, *J. Mater. Chem. A* **2014**, *2*, 13612 – 13623.
[10] W. Y. Teoh, J. A. Scott, R. Amal, *J. Phys. Chem. Lett.* **2012**, *3*, 629 – 639.
[11] M. Li, L. Zhang, X. Fan, Y. Zhou, M. Wu, J. Shi, *J. Mater. Chem. A* **2015**, *3*, 5189 – 5196.
[12] T. Nakamura, Y. Ling, K. Amezawa, *J. Mater. Chem. A* **2015**, *3*, 10471 – 10479.
[13] X. D. Zhou, J. W. Templeton, Z. Nie, H. Chen, J. W. Stevenson, L. R. Pederson, *Electrochim. Acta* **2012**, *71*, 44 – 49.
[14] D. Chen, R. Ran, K. Zhang, J. Wang, Z. Shao, *J. Power Sources* **2009**, *188*, 96 – 105.
[15] C. Xia, W. Rauch, F. Chen, M. Liu, *Solid State Ionics* **2002**, *149*, 11 – 19.
[16] Y. Orikasa, T. Ina, K. Yamamoto, T. Nakano, A. Mineshige, K. Amezawa, T. Kawada, H. Tanida, T. Uruga, Y. Uchimoto, *Electrochemistry* **2014**, *82*, 897 – 900.
[17] Y. Fujimaki, H. Watanabe, Y. Terada, T. Nakamura, K. Yashiro, S. Hashimoto, T. Kawada, K. Amezawa, *ECS Trans.* **2013**, *57*, 1925 – 1932.
[18] R. J. Woolley, B. N. Illy, M. P. Ryan, S. J. Skinner, *J. Mater. Chem.* **2011**, *21*, 18592 – 18596.
[19] W. C. Chueh, A. H. McDaniel, M. E. Grass, Y. Hao, N. Jabeen, Z. Liu, S. M. Haile, K. F. McCarty, H. Bluhm, F. E. Gabaly, *Chem. Mater.* **2012**, *24*, 1876 – 1882.
[20] Z. A. Feng, F. E. Gabaly, X. Ye, Z. X. Shen, W. C. Chueh, *Nat. Commun.* **2014**, *5*, 4374.
[21] D. N. Mueller, M. L. Machala, H. Bluhm, W. C. Chueh, *Nat. Commun.* **2015**, *6*, 6097.
[22] E. J. Crumlin, E. Mutoro, W. T. Hong, M. D. Biegalski, H. M. Christen, Z. Liu, H. Bluhm, Y. Shao-Horn, *J. Phys. Chem. C* **2013**, *117*, 16087 – 16094.
[23] D. F. Ogletree, H. Bluhm, E. D. Hebenstreit, M. Salmeron, *Nucl. Instrum. Methods Phys. Res. Sect. A* **2009**, *601*, 151 – 160.
[24] S. Ghosal, J. C. Hemminger, H. Bluhm, B. S. Mun, E. L. D. Hebenstreit, G. Ketteler, D. F. Ogletree, F. G. Requejo, M. Salmeron, *Science* **2005**, *307*, 563 – 566.
[25] B. Bozzini, E. Tondo, M. Prasciolu, M. Amati, M. K. Abyaneh, L. Gregoratti, M. Kishinova, *ChemSusChem* **2011**, *4*, 1099 – 1103.
[26] R. Oike, K. Amezawa, T. Nakamura, Y. Tamenori, K. Yashiro, T. Kawada, *Solid State Ionics* **2014**, *262*, 911 – 913.
[27] R. Oike, Y. Okamoto, T. Tokushima, T. Nakamura, K. Amezawa, *Electrochemistry* **2016**, *84*, 793 – 796.
[28] T. Nakamura, K. Yashiro, K. Sato, J. Mizusaki, *Solid State Ionics* **2009**, *180*, 368 – 376.
[29] J. M. Bassat, P. Odier, A. Villesuzanne, C. Marin, M. Pouchard, *Solid State Ionics* **2004**, *167*, 341 – 347.
[30] E. Boehm, J. M. Bassat, P. Dordor, F. Mauvy, J. C. Grenier, Ph. Stevens, *Solid State Ionics* **2005**, *176*, 2717 – 2725.
[31] E. Pellegrin, J. Zaanen, H. J. Lin, G. Meigs, C. T. Chen, H. Eisaki, S. Uchida, *Phys. Rev. B* **1996**, *53*, 10667 – 10679.
[32] Z. Hu, S. Golden, J. Fink, G. Kaindl, S. A. Warda, D. Reinen, P. Mahadevan, D. D. Sarma, *Phys. Rev. B* **2000**, *61*, 3739 – 3744.
[33] P. Kuiper, J. Elp, D. E. Rice, D. J. Buttrey, H. J. Lin, C. T. Chen, *Phys. Rev. B* **1998**, *57*, 1552 – 1557.
[34] T. Nakamura, R. Oike, Y. Ling, Y. Tamenori, K. Amezawa, *Phys. Chem. Chem. Phys.* **2016**, *18*, 1564 – 1569.
[35] W. Li, B. Guan, X. Zhang, J. Yan, Y. Zhou, X. Liu, *Phys. Chem. Chem. Phys.* **2016**, *18*, 8502 – 8511.
[36] T. Kawada, J. Suzuki, M. Sase, A. Kaimai, K. Yashiro, Y. Nigara, J. Mizusaki, K. Kawamura, H. Yugami, *J. Electrochem. Soc.* **2002**, *149*, E252 – E259.
[37] Y. Orikasa, T. Ina, T. Nakao, A. Mineshige, K. Amezawa, M. Oishi, H. Arai, Z. Ogumi, Y. Uchimoto, *J. Phys. Chem. C* **2011**, *115*, 16433.
[38] J. Suntivich, W. T. Hong, Y. L. Lee, J. M. Rondinelli, W. Yang, J. B. Goodenough, B. Dabrowski, J. W. Freeland, Y. Shao-Horn, *J. Phys. Chem. C* **2014**, *118*, 1856.
[39] T. Mizokawa, Y. Wakisaka, T. Sudayama, C. Iwai, K. Miyoshi, J. Takeuchi, H. Wadati, D. G. Hawthorn, T. Z. Regier, G. A. Sawatzky, *Phys. Rev. Lett.* **2013**, *111*, 056404.
[40] K. Luo, M. R. Roberts, N. Guerrini, N. T. -Ruiz, R. Hao, F. Massel, D. M. Pickup, S. Ramos, Y.-S. Liu, J. Guo, A. V. Chadwick, L. C. Duda, P. G. Bruce, *J. Am. Chem. Soc.* **2016**, *138*, 11211 – 11218.
[41] A. Yamada, Y. Suzuki, K. Saka, M. Uehara, D. Mori, R. Kanno, T. Kiguchi, F. Mauvy, J. C. Grenier, *Adv. Mater.* **2008**, *20*, 4124 – 4128.
[42] F. Mauvy, J. M. Bassat, E. Boehm, J. P. Manaud, P. Dordor, J. C. Grenier, *Solid State Ionics* **2003**, *158*, 17 – 28.
[43] Y. Tamenori, *J. Synchrotron Radiat.* **2010**, *17*, 243 – 249.

Manuscript received: February 9, 2017
Revised: March 16, 2017
Accepted Article published: March 16, 2017
Final Article published: April 13, 2017